On sonic anemometer measurement theory

Alvaro Cuerva / Angel Sanz-Andrés

Abstract

In this paper a model for the measuring process of sonic anemometers (ultrasound pulse based) is presented. The differential equations that describe the travel of ultrasound pulses are solved in the general case of non-steady, non-uniform atmospheric flow field. The concepts of instantaneous line-average and travelling pulse-referenced average are established and employed to explain and calculate the differences between the measured turbulent speed (travelling pulse-referenced average) and the line-averaged one. The limit $k_1 l = 1$ established by Kaimal in 1968, as the maximum value which permits the neglect of the influence of the sonic measuring process on the measurement of turbulent components is reviewed here.

Three particular measurement cases are analysed: A non-steady, uniform flow speed field, a steady, non-uniform flow speed field and finally an atmospheric flow speed field. In the first case, for a harmonic time-dependent flow field, Mach number, M (flow speed to sound speed ratio) and time delay between pulses have revealed themselves to be important parameters in the behaviour of sonic anemometers, within the range of operation. The second case demonstrates how the spatial non-uniformity of the flow speed field leads to an influence of the finite transit time of the pulses ($M \neq 0$) even in the absence of non-steady behaviour of the wind speed. In the last case, a model of the influence of the sonic anemometer processes on the measurement of wind speed spectral characteristics is presented. The new solution is compared to the line-averaging models existing in the literature. Mach number and time delay significantly distort the measurement in the normal operational range. Classical line averaging solutions are recovered when Mach number and time delay between pulses go to zero in the new proposed model.

The results obtained from the mathematical model have been applied to the calculation of errors in different configurations of practical interest, such as an anemometer located on a meteorological mast and the transfer function of a sensor in an atmospheric wind.

*Corresponding author. Tel.: +34-91-346-6039; fax: +34-91-346-6037.
E-mail address: cuerva@ciemat.es (A. Cuerva).

0167-6105/00/$ - see front matter
PII: S0167-6105(00)00023-4

The expressions obtained can be also applied to determine the quality requirements of the flow in a wind tunnel used for ultrasonic anemometer calibrations.

Keywords: Sonic anemometers; Atmospheric turbulence measurement; Models

Nomenclature

c	Sound speed (ms^{-1})
d	sonic path met. mast support diameter (m)
f	frequency of the flow speed (Hz)
$\boldsymbol{i}_p$	unit vector along the measurement path
$\boldsymbol{j}_p$, $\boldsymbol{k}_p$	unit vectors configuring a right-hand defined reference system with $\boldsymbol{i}_p$ (path aligned reference system)
$\boldsymbol{i}_w$	unit vector along the mean atmospheric wind speed
$\boldsymbol{j}_w$, $\boldsymbol{k}_w$	unit vectors configuring a right-hand defined reference system with $\boldsymbol{i}_w$ (mean wind reference system)
$\boldsymbol{k}$	wave number (m^{-1})
l	path length (m)
l_w	representative length scale of flow variation (m)
p	pulse position referred to a reference point of the measuring path (m)
p_i	path extremes. $i=1, 2$ (m)
t_{ij}	total flight time for a pulse to travel from path extreme i to j. $ij=12$, 21 (s)
t_r	reference time (s)
$\boldsymbol{u}$	flow speed vector (ms^{-1})
u_p	flow speed component parallel to the path (ms^{-1})
u_r	reference flow speed (modulus) (ms^{-1})
u_n	flow speed component perpendicular to the path (ms^{-1})
u_i	atmospheric wind speed component expressed in mean speed reference system (ms^{-1})
u_p^M	measured flow speed component along the path (ms^{-1})
u_i^M	measured atmospheric flow speed component expressed in wind axis (ms^{-1})
u_x	instantaneous space average of $u_p(p, t)$ (ms^{-1})
$\boldsymbol{u}_\infty$	atmospheric mean wind speed vector (ms^{-1})
$\hat{u}_i$	atmospheric wind speed turbulent component expressed in mean speed reference system (ms^{-1})
$\boldsymbol{x}$	centre of the measuring path (m)
z_B	time delay between pulses (s)
E	three-dimensional energy spectrum of turbulence (m^3s^{-2})
F^+	positive travelling pulse referenced average of the perturbation flow speed defined by Eq. (19)

F^-	negative travelling pulse referenced average of the perturbation flow speed defined by Eq. (22)
F_{ij}	one-dimensional spectral density tensor
F_{ij}^{M}	measured one-dimensional spectral density tensor
H_{p}	non-dimensional difference between measured flow speed along the path and reference flow speed
M	mach number
M_{r}	mach number based on reference flow speed
P_i	path extremes ($i=1$, 2.)
R_{ij}	ratio of measured to actual one-dimensional spectral density tensors
T_{ij}	dimensionless total flight time for a pulse to travel from path extreme i to j ($ij=12$, 21)
T^+	dimensionless time, function of the pulse position, travelling from path extreme 1 to 2
T^-	dimensionless time, function of the pulse position, travelling from path extreme 2 to 1
T_0	dimensionless time delay between the flow field and the pulse shot
$U_{\mathrm{p}}^{\mathrm{M}}$	measured flow speed component along the path (non-dimensional)
Z_{B}	dimensionless time delay between pulse shots
δ	dimensionless perturbation component of the flow speed along the path
ε	scaling factor for flow speed perturbation component
$\in$	rate of turbulent energy dissipation. ($\mathrm{m}^2\ \mathrm{s}^{-3}$)
φ_{12}	phase angle between harmonic wind speed and shooting time for pulse 1-2 (rad)
φ_{21}	phase angle between harmonic wind speed and shooting time for pulse 2-1 (rad)
ω	angular frequency for a uniform and non-steady flow speed field (rad/s)
Φ_{ij}	spectral density tensor ($\mathrm{m}^5\ \mathrm{s}^{-2}$)
Φ_{ij}^{M}	measured spectral density tensor ($\mathrm{m}^5\ \mathrm{s}^{-2}$)
Ψ_i^{M}	random functions to define component along $\boldsymbol{i}_{\mathrm{w}}$ of measured atmospheric wind speed vector ($\mathrm{m\ s}^{-1}$)
Ψ_i	random functions to define component along $\boldsymbol{i}_{\mathrm{w}}$ of atmospheric wind speed vector ($\mathrm{m\ s}^{-1}$)
Ω	angular frequency for a uniform and non-steady flow speed field
$\Delta(x)$	increment $x_2 - x_1$ (m)

1. Introduction

Since their pioneer utilisation in atmospheric flow studies in the 1950s [1], sonic anemometers have shown themselves to be the most suitable instruments to measure atmospheric turbulent flows, see Ref. [2].

Extensively used in meteorological and pollution studies, [3], sonic anemometers have become widely used in Wind Energy and Civil Aerodynamics applications.

These sensors are able to measure deterministic and stochastic characteristics of the wind speed vector at one point, that drive the loading state of large structures (wind turbines, bridges or buildings) or their power performance in case of wind turbines. Thus, they allow valid information to be obtained to optimise aerodynamic and structural design. In Ref. [4], anemometers are used to obtain flow characteristics in urban areas in Japan. In Ref. [5], flow parameters obtained from sonic anemometer measurements are used in models that describe wind turbine structural and energetic response. Furthermore, recent research projects within the European framework are taking advantage of this technology to open up new design methods, once a better knowledge of flows is achieved (mostly in complex terrain). See Refs. [6,7].

The advantages of sonic anemometers versus other outdoor instruments have often been reviewed in different works. Thus, in Refs. [8,2], these advantages are listed as follows:

1. The absence of moving parts that have to get into dynamic equilibrium with the flow, therefore problems such cup anemometer overspeeding (over estimation of wind speed in turbulent flow) do not appear, see Refs. [9,10].
2. Sonic anemometers have a linear response in a wide range of frequencies, although this hypothesis is reviewed in the present work. They are absolute instruments and their calibration parameters are fixed once they are constructed.
3. The measurement is relatively independent of the flow properties (spatial and time variations, density, temperature, etc). This hypothesis is revisited in this paper.

A comparison between different technologies to measure atmospheric flows, including economic and operational aspects, can be found in Ref. [11]. Again, sonic anemometers turn out to be the preferred choice.

In addition to their advantages, sonic anemometers also present some drawbacks that affect the measurement. These problems along with the different designs that exist in the market actually make it difficult to systematise their usage.

Following Ref. [8], the main deficiencies are the effect of finite path (line averaging), path separation and transducer shadows.

In this paper a basic approach to sonic anemometry measurement is presented based on the modelling of the process by means of the differential equations that describe the motion of ultrasound pulses in a non-steady and non-uniform media.

First, the presently used measuring algorithm is introduced and reviewed, than the mathematical model for sound pulse propagation is presented, and the solution for the general atmospheric case and some interesting particular problems such as uniform, non-steady and steady, non-uniform velocity fields and atmospheric turbulent flow are considered. Applications of the mathematical model results to some practical cases are presented (anemometer on oscillating met. mast and atmospheric flow).

The results established in the literature are recovered as simplified cases of the general model presented here.

2. Principle of operation and measuring algorithm

All sonic anemometers (pulse based) present the same principle of operation. They measure flow speed by measuring the influence of this magnitude in the time of flight of ultrasound pulses, that travel between pairs of transmitters and receivers. Each of these pairs configures a measuring path.

However, there has been an evolution of their design with time, mostly due to electronic device improvements. Thus, original models as the EG&G-198-3 described in Ref. [2]; that required a couple of transmitters and receivers in each measuring path, have been replaced by models such as the Gill Wind Master described in Ref. [12], where each measuring path is configured by only two sensors that carry out the functions of transmitter and receiver simultaneously.

In Ref. [13], sensors of both technologies are investigated. These two types of design generally have two different algorithm associated with them. The main difference between them consists in the influence that sound speed (i.e. air temperature and moisture) typically has on the measuring algorithm.

In the first case, Fig. 1a, due to less sophisticated electronics, that does not allow the calculation of flight time inverses (as it is later explained) the squared sound speed appears directly in the measuring algorithm, see expression (1). This limitation also leads to larger sampling times.

As is described in several references (i.e. Ref. [2]) the first algorithm is represented by the following formulae:

$$u_{\mathrm{p}}^{\mathrm{M}} = \frac{c^2}{2l}\,\Delta t, \tag{1}$$

where $\Delta t = t_{12} - t_{21}$. t_{ij} is the time of flight from transmitter "i" to receiver "j".

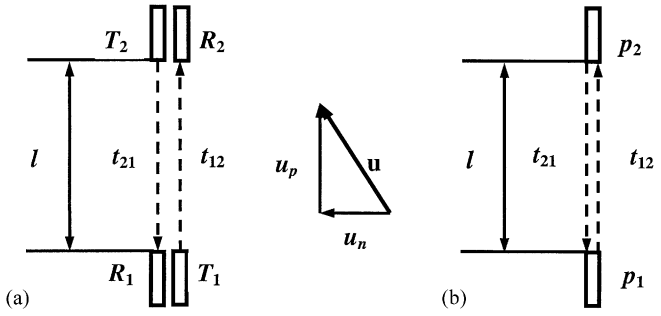

Fig. 1. Schematic of the two different sonic path designs.

In the other case [14], the electronics allow the calculation of flight time inverses, the algorithm being the following:

$$u_{\mathrm{p}}^{\mathrm{M}} = \frac{l}{2}\,\Delta\left(\frac{1}{t}\right), \tag{2}$$

where $\Delta(1/t) = 1/t_{12} - 1/t_{21}$.

Both expressions (1) and (2) are valid in the case of a steady-uniform flow field. However, some doubts are cast concerning their correctness in non-steady or non-uniform flow fields.

In Ref. [2], it is also proved that wind speed component normal to the measuring path does not have any influence, in the first approximation, on the measuring process, if $u \ll c$. This point will be generally reviewed in this paper, and the order of magnitude of the error associated with this assumption obtained.

Both algorithms are quite simplified models of the real process that actually is going on. A further and more complete interpretation of the sonic measuring mechanism is presented in Refs. [15–17]. These authors basically apply a "Line-averaging" model for the case of atmospheric-flow measurement. Therefore the measured turbulent wind speed vector components are obtained from the original ones by spatially averaging them along a measuring path (see Ref. [15], expression (10)) as given by

$$u_i^{\mathrm{M}}(\boldsymbol{x}, l) = \frac{1}{l}\int_{-l/2}^{l/2} \hat{u}_i(\boldsymbol{x} + \boldsymbol{s})\,\mathrm{d}s. \tag{3}$$

The result is that a sonic anemometer behaves as a directional low-pass filter which produces some attenuation of wind speed for some specific wave numbers, $\boldsymbol{k}$, i.e. combinations of wind speed frequencies and mean wind speed.

However, in the previously described "Line-averaging" models the turbulent flow is considered as completely frozen and therefore not changing with time during pulse travels.

In the following sections, space and time variations of flow speed are considered in a review of the "Line-averaging" model, by setting up and solving the appropriate differential equations. These equations describe the flight of an ultrasound pulse that travels along a measuring path, that is immersed in a non-steady and non-uniform wind speed field. Afterwards, the results are applied to the atmospheric case in order to establish comparisons with results from Ref. [15].

Results are obtained for a general non-steady, non-uniform case as well as a particularisation for a non-steady, uniform flow and non-uniform steady flow. The second case is finally represented by a harmonic time-dependent flow speed and an example of the response of the instrument mounted on an oscillating met. mast, for two commercial sonic anemometer paths is included.

The new approach enables the influence of finite time travel of the pulses in terms of the Mach number to be obtained. The predicted correction in measured atmospheric flow spectra in certain conditions is significant. In the case of Mach number 0 (which means that sound speed can be considered infinite versus reference wind speed) the "Line-averaging" model results are recovered.

3. Mathematical model of the ultrasound pulse flight

In this part, the mathematical model that describes the ultrasound pulse flight is presented and the solution is obtained in an asymptotic case, via a perturbation method in Section 4. Only the algorithm based on time inverses is considered here.

It is assumed that pulses from transmitter 1 to receiver 2 and from transmitter 2 to receiver 1, are simultaneously shot. Should any delay between path shots occur then distortions in the measurement will arise. This will be considered in Section 5.1 and in the atmospheric case example in Section 7. In the same way, both the delay between shots in different paths and their sampling, influence the measurements as it is proved in Ref. [18], in a study on a Gill Research model. In the cited paper this effect is described via two attenuation terms.

Finally it is assumed that pulses follow the line of the path, thus, the measurement is practically unaffected by lateral speed components if $M = u_r/c \ll 1$ (See the appendix and Ref. [2]).

The flying times for the simultaneous pulses are given by the following equations:

$$t_{12} = \int_{p_1}^{p_2} \frac{\mathrm{d}p}{c + u_p(p,t)}, \tag{4a}$$

$$t_{21} = \int_{p_2}^{p_1} \frac{\mathrm{d}p}{-c + u_p(p,t)}, \tag{4b}$$

where c is the sound speed, $u_p(p,t)$ is the value of the wind speed component along the path, in a specific point p of the path for a given time t. p_1 and p_2 represent the two extremes of the path. The following non-dimensional variables will be used:

$$T = t\frac{u_r}{l}, \quad P = \frac{p}{l}, \quad M_r = \frac{u_r}{c}, \quad U^M = \frac{u^M}{u_r}, \tag{5}$$

where u_r is a suitable reference wind speed that can be a time- or space- (along the path) averaged value, depending on the case, l is the path length, and M_r is the Mach number based on the previously defined reference wind speed. u^M and U^M are the dimensional and dimensionless flow speeds, respectively, measured by the anemometer according to algorithm (2). Eqs. (4a) and (4b) in non-dimensional form result

$$T_{12} = M_r \int_{P_1}^{P_2} \frac{\mathrm{d}P}{1 + M_r\,(u_p(P,T)/u_r)}, \tag{6a}$$

$$T_{21} = M_r \int_{P_2}^{P_1} \frac{\mathrm{d}P}{-1 + M_r\,(u_p(P,T)/u_r)}, \tag{6b}$$

If the actual velocity field was known and once these integrals were accordingly calculated, the flow speed measured by the anemometer, u_p^M, as given by

algorithm (2) would be in dimensionless form

$$U_{\mathrm{p}}^{\mathrm{M}} = \frac{l}{2u_{\mathrm{r}}}\,\Delta\left(\frac{1}{t}\right) = \frac{1}{2}\,\Delta\left(\frac{1}{T}\right) = \frac{1}{2}\left[\left(\frac{1}{T_{12}}\right) - \left(\frac{1}{T_{21}}\right)\right]. \tag{7}$$

The relative difference between the measurement and the reference value, H_{p}, is defined as follows:

$$H_{\mathrm{p}} = \frac{u_{\mathrm{p}}^{\mathrm{M}} - u_{\mathrm{r}}}{u_{\mathrm{r}}}. \tag{8}$$

4. Solution of the equations

Eqs. (6a) and (6b) can be used to calculate T_{12} and T_{21} in terms of some specific flow speed averages. To do this the flow speed field along the path is defined as a summation of a reference value, that is constant u_{r}, plus a small perturbation component which is a function of time and position along the path, $\varepsilon u_{\mathrm{r}}\delta(p,t)$,

$$u_{\mathrm{p}}(p,t) = u_{\mathrm{r}}(1 + \varepsilon\delta(p,t)), \tag{9}$$

where $\varepsilon \ll 1$ denotes the order of magnitude of the perturbation. It must be noted that spatial co-ordinate p is relative to the path origin and directed along it. Once the flow speed field is defined, the Eqs. (6a) and (6b) can be rewritten, by using Eq. (9), in differential form and in terms of dimensionless variables as follows. Let us denote $\mathrm{d}T^{+}(P)$ the time needed for the pulse at point P to move a non-dimensional distance $\mathrm{d}P$ in the p_1–p_2 direction ($P_1 = 0$, $P_2 = 1$)

$$\mathrm{d}T^{+} = \frac{M_{\mathrm{r}}/(1 + M_{\mathrm{r}})\;\mathrm{d}P}{1 + M_{\mathrm{r}}/(1 + M_{\mathrm{r}})\;\varepsilon\delta(P,T)} \tag{10a}$$

with conditions.

$$T^{+}(0) = 0, \quad T^{+}(1) = T_{12}. \tag{10b}$$

The problem defined by Eqs. (10a) and (10b) can be solved by using perturbation methods. The function $T^{+}(P)$ is considered as a summation of a first-order term plus a term of the same order as the flow speed perturbation

$$T^{+}(P) = T_0^{+}(P) + \varepsilon T_1^{+}(P). \tag{11}$$

As $0 < M_{\mathrm{r}} \ll 1$, the term $M_{\mathrm{r}}/(1 + M_{\mathrm{r}})$ is valued between 0 and 1 and therefore the term $\varepsilon\delta(P,T)M_{\mathrm{r}}/(1 + M_{\mathrm{r}}) \ll 1$. Thus, considering this and introducing expansion (11) into Eq. (10a) gives

$$\mathrm{d}T_0^{+}(P) + \varepsilon\,\mathrm{d}T_1^{+}(P) = \frac{M_{\mathrm{r}}}{1 + M_{\mathrm{r}}}\left(1 - \frac{\varepsilon M_{\mathrm{r}}}{1 + M_{\mathrm{r}}}\,\delta(P,T)\right)\mathrm{d}P + \mathrm{O}(\varepsilon^2 M_{\mathrm{r}}). \tag{12}$$

Eq. (12) can be split into two problems, one for each order:

$$\mathrm{d}T_0^{+}(P) = \frac{M_{\mathrm{r}}}{1 + M_{\mathrm{r}}}\,\mathrm{d}P, \quad T_0^{+}(0) = 0, \tag{13a}$$

$$\mathrm{d}T_1^+(P) = -\frac{M_r^2}{(1+M_r)^2}\,\delta(P,T)\,\mathrm{d}P,\; T_1^+(0) = 0. \tag{13b}$$

Finally, once both problems are solved, the flying time T_{12} can be expressed as follows:

$$T_{12} = T^+(1) = T_0^+(1) + \varepsilon T_1^+(1). \tag{14}$$

The solution for the first problem Eq. (13a) is

$$T_0^+(P) = \frac{M_r}{1+M_r}\,P. \tag{15}$$

To solve problem (13b) expression (11) is substituted in the expression of $\delta(P,T)$:

$$\begin{aligned}\delta(P,T) &= \delta(P,T(P)) = \delta(P,T^+(P)) = \delta(P,T_0^+(P)+\varepsilon T_1^+(P))\\ &\approx \delta(P,T_0^+(P)) + \mathrm{O}(\varepsilon).\end{aligned} \tag{16}$$

Furthermore, Eq. (13b) can be solved by using Eqs. (15) and (16), obtaining

$$T_1^+(P) = -\frac{M_r^2}{(1+M_r)^2}\int_0^P \delta(P,T_0^+(P))\,\mathrm{d}P. \tag{17}$$

Finally expressions (15) and (17) introduced in Eq. (14) giving the total ultrasound pulse flight time, travelling from p_1 to p_2:

$$T_{12} = \frac{M_r}{1+M_r}\left(1 - \frac{M_r}{1+M_r}\,\varepsilon F^+\right), \tag{18}$$

where F^+ is defined as follows:

$$F^+ = \int_0^1 \delta(P,T_0^+(P))\,\mathrm{d}P. \tag{19}$$

F^+ represents, in a first approximation, the average of the perturbation field as seen by the travelling pulse from p_1 to p_2 (pulse-referenced average).

The corresponding equation for the pulse travelling from p_2 to p_1 is

$$\mathrm{d}T^- = -\frac{M_r/(1-M_r)\,\mathrm{d}P}{1 - M_r/(1-M_r)\,\varepsilon\delta(P,T)},\; T^-(1) = 0,\; T^-(0) = T_{21}. \tag{20}$$

In this case the assumption $\varepsilon\delta(P,\ T)M_r/(1-M_r) \ll 1$ is not so general since for M_r close to 1, this term can grow up to infinity. For this case we will assume that the term $M_r/(1-M_r)$ remains between 0 and 1 which implies M_r ranging from 0 to 0.5. This interval covers perfectly the common range of usage of sonic anemometers.

Using a similar procedure to that presented above for the calculation of the travel time from p_2 to p_1, the following expression is obtained:

$$T_{21} = \frac{M_r}{1-M_r}\left(1 + \frac{M_r}{1-M_r}\,\varepsilon F^-\right), \tag{21}$$

where F^- is defined by

$$F^- = \int_0^1 \delta(P,\ T_0^-(P))\,\mathrm{d}P \tag{22}$$

and $T_0^-(P)$ is the time to reach the point P obtained from the first-order problem as in Eq. (15)

$$T_0^-(P) = \frac{M_r}{1 - M_r}(1 - P). \tag{23}$$

The physical meaning of F^- is the same as of F^+, but for the pulse travelling from p_2 to p_1. U_p^M is obtained by introducing Eqs. (18) and (21) into Eq. (7):

$$U_p^M = 1 + \tfrac{1}{2}\varepsilon(F^+ + F^-) + O(\varepsilon^2). \tag{24}$$

It must be noted that the obtained solution is valid up to ε order terms. The dimensional magnitude for u_p^M is

$$u_p^M = u_r\,[1 + \tfrac{1}{2}\,\varepsilon\,(F^+ + F^-)]. \tag{25}$$

Introducing Eq. (25) in Eq. (8), the relative difference between measured and reference flow speed, H_p is obtained in terms on F^+ and F^-:

$$H_p = \tfrac{1}{2}\,\varepsilon(F^+ + F^-). \tag{26}$$

It should be noted that, considering these results, a sonic anemometer does not measure really the instantaneous-averaged wind speed as it is generally supposed. On the contrary, the measurement is biased by the turbulent component or other perturbation existing in the flow speed, represented here by the term $\varepsilon(F^+ + F^-)/2$.

Observe that in a first order, the difference H_p does depend on the Mach number through T_0^+ and T_0^- functions in F^+ and F^-. Eqs. (24) and (25) show that if either ε or $F^+ + F^-$ vanishes, the measured wind speed u_p^M equals the reference wind speed u_r. Otherwise, differences will arise. In order to explain the previous statements, let u_x be the instantaneous line average of $u_p(p, t)$ along the path at $t = 0$, then

$$u_x = \frac{1}{l}\int_0^l u_r\,[1 + \varepsilon\delta(p, 0)]\,\mathrm{d}p = u_r + \varepsilon\,\frac{1}{l}\int_0^l \delta(p, 0)\,\mathrm{d}p. \tag{27}$$

It should be remembered that time t is relative to the shooting instant. Let us assume that u_r is chosen in such a way that the instantaneous space average of the perturbation (the integral in the right-hand side) is zero, thence $u_x = u_r$. On the other hand, observe that the correction terms F^+ and F^- represent the averaged flow speed as seen by the positive$^+$ and negative$^-$ going travelling pulses, respectively, which would not vanish in a general case, and therefore the measured speed will be different from the instantaneous space average, $u_p^M \neq u_r = u_x$. However, if the perturbation $\delta(p,\ t)$ is known then F^+ and F^- can be used, at least, to estimate the uncertainties in the anemometer measurements. Atmospheric flow constitutes an interesting case where the error in the measurement is obtained as a function of the wave number $\boldsymbol{k}$. In general it can be stated that u_p^M will differ from the instantaneous line average.

It must be also noted that Mach number dependency also makes that u_p^M depends on temperature, humidity and the composition of fluid we are measuring since $M_r = u_r/\sqrt{\gamma RT}$, where R and γ are specific gas constant and adiabatic constant of the gas, respectively. More exact models include a dependency of Mach number on humidity. This dependency, traditionally associated with sonic

anemometers based on algorithm (1) [20] due to its direct dependency on sound speed, also will appear in anemometers that use Eq. (2) but as a correction of the correction.

5. Uniform and non-steady speed field

The objective of this section is twofold. First it aims to show the influence of time variation of flow speed during the pulse transmission in an otherwise uniform flow. A second objective is its application to a real case, i.e. the flow experienced by an anemometer mounted on the top of a met. mast presenting transverse oscillation induced by vortex shedding (normal case in wind energy and meteorology application) or by an anemometer located in the vortex wake of an obstacle. If one makes the assumption that $l/l_w \ll 1$, where l_w is a typical length scale of the flow, then the flow field experienced by the path can be considered as a non-steady, uniform one, and this formulation is directly applicable. Other cases where it can be used is in the study of the effects of mechanical vibration of an anemometer around its equilibrium position (due to sensor flexibility) or to define the requirements of flow quality for calibration wind tunnels.

In this case the pulse-referenced averages F^+ and F^- that appear in Eqs. (19) and (22) have to be expressed in the time variable T. Moreover the function $\delta(P, T)$ depends exclusively on T, being $\delta = \delta(T^+)$ for the flight from p_1 to p_2 and $\delta = \delta(T^-)$ from the flight from p_2 to p_1.

Using solutions (15) and (23), valid in first approximation to define $T_0^{\pm}(P, T) \equiv T_0^{\pm}(P)$, F^+ and F^- expressions result:

$$F^{\pm} = \int_0^1 \delta(P, T_0^{\pm}(P))\, \mathrm{d}P = \int_0^{T_0^{\pm}(1)} \delta(T_0^{\pm}) \frac{1 \pm M_r}{M_r}\, \mathrm{d}T_0^{\pm}$$
$$= \frac{1 \pm M_r}{M_r} \int_0^{M_r/(1 \pm M_r)} \delta(T)\, \mathrm{d}T. \tag{28}$$

This expression helps to explain the physical meaning of F^+ and F^-, i.e. in an uniform field they are proportional to the time average of the perturbation along the time of flight.

Observe that the only differences between the integrals in F^+ and F^- are the upper integration limits which implies that the integration time for $+$ direction pulse is shorter than the time for $-$ travel one.

5.1. *Harmonic time-dependent flow speed*

In order to illustrate the case of uniform and non-steady flow field, a sinusoidal variation of wind speed around an averaged value will be considered here. Let the perturbation $\delta(t)$ be defined as

$$\delta(t) = \sin(\omega t + \varphi) = \sin(\Omega T + \varphi), \tag{29}$$

where ω and Ω are the dimensional and non-dimensional ($\Omega = \omega l/u_r$) angular frequency, respectively, and φ is a phase angle that indicates the delay between the flow speed and the pulse shooting instants.

Introducing Eq. (29) into Eq. (28) one can obtain the expressions for $F^{\pm}$ in terms of the reference Mach number, M_r, and the phase angle φ:

$$F^{\pm} = \frac{1 \pm M_r}{\Omega M_r}\left[\cos\varphi - \cos\left(\frac{\Omega M_r}{1 \pm M_r} + \varphi\right)\right] \approx \sin\varphi + \frac{\Omega M_r}{1 \pm M_r}\frac{\cos\varphi}{2}. \tag{30}$$

The last expression is valid in the case $\Omega M_r \ll 1$. Both F^+ and F^- have the same sign, and are roughly of the same amount, the difference between them being of the order of ΩM_r^2.

Finally, by introducing expressions (30) in Eq. (24) the expression of U_p^M in terms of M_r and φ is obtained:

$$U_p^M \approx 1 + \varepsilon \sin\varphi + \frac{1}{2}\varepsilon M_r \Omega \cos\varphi. \tag{31}$$

The difference between u_p^M and u_r given by Eq. (31) depends on the perturbation relative amplitude ε, the delay phase φ, the Mach number M_r and the angular frequency Ω.

In the calculation of Eq. (31) by means of Eq. (28) it is implicit that the measurement process takes place at $t = 0$. However the result has general application because the difference in phase between measurement process and flow speed is taken into account by φ. In the case considered, u_r represents the long-term-averaged value of $u_p(t)$. Nevertheless, in the short term, the actual speed is $u_p(0)$, that is

$$u_p(0) = u_r(1 + \varepsilon \sin\varphi) \tag{32}$$

and, thus, the relative speed difference H_p should be redefined in terms of the actual speed $u_p(0)$ as follows:

$$H_p = \frac{U_p^M - U_p(0)}{U_p(0)} \approx \frac{1}{2}\varepsilon M_r \Omega \cos\varphi = \frac{1}{2}\varepsilon M_r \Omega \cos(\Omega T_0), \tag{33}$$

where T_0 is the non-dimensional time delay, being $\varphi = \Omega T_0$.

Observe that the difference between instantaneous and measured wind speeds is proportional to εM_r. If the phase remains constant, the error depends linearly on the frequency Ω.

The effect of the phase appears through the factor $\cos\varphi \propto \dot{\delta}(0)$. The meaning is rather clear: if the pulse is shot when the perturbation field is passing through a maximum or a minimum, $\dot{\delta}(0) = 0$, the error vanishes. The maximum error occurs when the acceleration is a maximum, $\ddot{\delta}(0) = 0$ (that is $\sin\varphi = 0$).

Results obtained from Eq. (33) are shown in Fig. 2, where a constant time delay T_0 instead a constant phase has been considered. Observe that the amount of error can be noticeable for Ω larger than 1 (see Ref. [15]), and that the error vanishes when $\varphi = 2\pi f t_0$ is an odd multiple of $\pi/2$.

Note that $\Omega = 1$ typically corresponds to $\omega = 100$ rad/s ($l = 0.1$ m, $u_r = 10$ m/s) that is a frequency $f \approx 16$ Hz. In dimensional form Eq. (33) can be expressed as

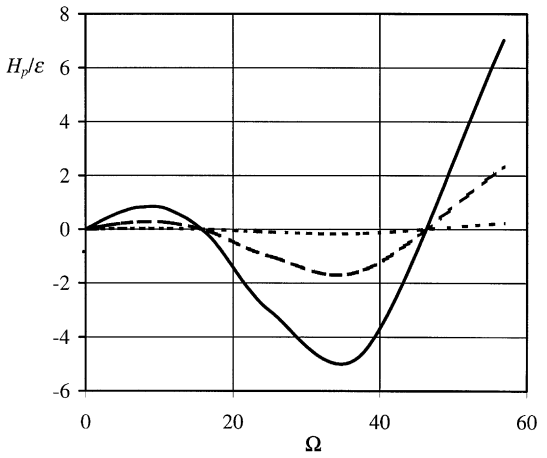

Fig. 2. Variation of the relative error H_p with the dimensionless frequency Ω (uniform non-steady flow field case). The phase is $\varphi = \Omega T_0$, $T_0 = 0.1$. Short dashed line: $M_r = 0.001$, large dashed line: $M_r = 0.1$, solid line: $M_r = 0.3$. M_r is the Mach number.

follows:

$$u_p(0) = u_p^M \left(1 + \frac{1}{2}\varepsilon \frac{2\pi f\, l}{c} \cos(2\pi f\, t_0)\right)^{-1}. \tag{34}$$

If the magnitude of ε, f, t_0 and c were known then the error could be calculated and the true instantaneous speed $u_p(0)$ could be determined from the measured speed u_p^M. Actually, an estimation of ε, ω, φ can be performed by analysing a record of measurements containing several periods of the flow speed variation. c can be determined from the measured temperature. Observe that if the measurements are evenly distributed along an entire number of cycles (coherent sampling without any leakage) the average of the speed measurement u_p^M coincides with the average speed u_r, because the average of errors (the same as the average of cos φ) vanishes.

The previous results correspond to a simultaneous emission of the pulses. The case of some delay between the shooting of the pulses is equivalent to consider two delays, φ_{12} and φ_{21}, respectively, for each pulse. The contribution to the measurement is evaluated to be (in the case $M_r \ll 1$):

$$\begin{aligned} U_p^M &\cong 1 + \frac{\sin\varphi_{12} + \sin\varphi_{21}}{2} \\ &\approx 1 + \varepsilon \sin\varphi_{12} + \frac{\varepsilon}{2}\Delta\varphi \cos\varphi_{12} + O(\varepsilon(\Delta\varphi)^2). \end{aligned} \tag{35}$$

The last expression is valid if $\Delta\varphi = \varphi_{12} - \varphi_{21} \ll 1$, which could be a practical situation; otherwise it could significantly contribute to the error in the mean speed. In addition to that, a new definition of H_p is needed, because the actual speed at $t = 0$

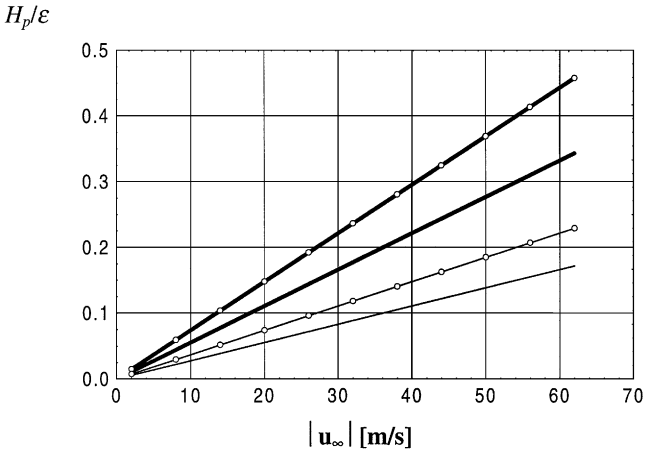

Fig. 3. Influence of met. mast oscillation induced by vortex shedding in the error of the turbulent flow speed measurements. Thick lines: $d=0.05$ m, thin lines: $d=0.1$ m. Dotted lines: Kaijo-Denki path, ($l=0.20$ m); otherwise: Gill WindMaster path, ($l=0.15$ m).

is $u_p(0)=u_r(1+\varepsilon \sin \varphi_{12})$

$$H_p=\frac{u_p^M-u_p(0)}{u_p(0)}=\frac{\varepsilon}{2}\Delta\varphi \cos \varphi_{12}+O(\varepsilon^2\Delta\varphi). \tag{36a}$$

It means that the error has a maximum value at $\varphi_{12}=0$, but the error vanishes, $H_p=0$, if the phase $\varphi_{12}=\pi/2$. In this last case, pulse emission occurs when there is no variation of speed with time, and therefore, the effect of a small phase difference $\Delta\varphi$ is minimised. In a practical situation ($\omega \approx 100$ rad/s, delay between pulses $t_0=2\times10^{-3}$ s, $\varphi_{12}\approx0$, $\varepsilon\approx0.1$, $\Delta\varphi=\omega t_0\approx200\times10^{-3}=0.2$) the error H_p, would be some 10^{-2}.

Fig. 3 illustrates the uniform, non-steady case by considering two types of commercial anemometer paths with different lengths, mounted on a met. mast oscillating due to vortex shedding induced by U_∞, a uniform-steady flow speed field. The shedding frequency in terms of the reduced frequency ($2\pi fd/U_\infty$) is considered to be 0.4π. ε, in this case, is the amplitude of the oscillation velocity at the path location. The path is situated orthogonal to the met. mast and forming a 45° angle with flow speed vector. The result is expressed in terms of H_p (33) divided by ε:

$$\frac{H_p}{\varepsilon}=0.2\pi\, M_r\frac{l}{d}. \tag{36b}$$

In order to facilitate the analysis the phase delay term t_0 is considered 0. In these conditions, the relative error H_p/ε is linearly dependent on both the ratio l/d and M_r which means that for given flow conditions (c defined) this relative error depends linearly on U_r. The analysis for a specific path and flow speed shows that the smaller the diameter the larger the error. This is due to the fact that smaller diameter implies larger frequency of oscillation, and therefore a larger number of cycles of wind speed

within the path. A similar argument can be applied to the influence of the path length. The consideration of the trigonometric term of Eq. (33) introduces a strong non-linear behaviour of the relative error term versus flow velocity.

As shown in Fig. 3, in a practical case the relative error could amount to about 0.3 ε.

6. Steady-non-uniform flow speed field

By introducing Eq. (9), with $\delta(p,t) \equiv \delta(p)$, in Eqs. (6a) and (6b) the effect of the non-uniformity of an otherwise steady flow is obtained to be

$$\frac{u_{\mathrm{p}}^{\mathrm{M}}}{u_{\mathrm{r}}} = 1 + M_{\mathrm{r}}^2 \, (\varepsilon^2 \overline{\delta^2} + \varepsilon^3 \overline{\delta^3}) + \mathrm{O}(\varepsilon^2 M_{\mathrm{r}}^4), \tag{37}$$

where

$$\overline{\delta^n} = \frac{1}{l} \int_0^l \delta^n(p) \, \mathrm{d}p. \tag{38}$$

In Eq. (37) it has been assumed $\bar{\delta} = 0$ and therefore the reference speed u_{r} coincides with the path-averaged speed $\overline{u_{\mathrm{p}}}$. However, as shown by Eq. (37), even in this case there is a difference between the measured wind speed and the path-averaged speed u_{r} due to the flow spatial non-uniformity. The error term (or correction to be taken into account), $M_{\mathrm{r}}^2(\varepsilon^2 \overline{\delta^2} + \varepsilon^3 \overline{\delta^3})$, is of order 10^{-4} in typical applications ($M_{\mathrm{r}} \approx 0.1$, $\varepsilon^2 \overline{\delta^2} \approx 0.01$, $\varepsilon^3 \overline{\delta^3} \approx 0$).

As a consequence the sonic anemometer appears as very appropriate instrument to measure mean wind speed in steady flows even though they present significant non-uniformity. This feature is very different from the case of cup anemometers, where flow non-uniformity values lower than 0.2% are mandatory for calibration in a wind tunnel [21].

7. The case of atmospheric measurements

The measurement of atmospheric flows constitutes a typical case of measurement in a simultaneously non-uniform and non-steady flow speed field. In Ref. [15] as well as in Ref. [17], the effect of the measuring process of a sonic anemometer is described by a line-averaging effect that provokes significant deviations in power spectra estimations. Following these papers the measured wind speed components are obtained from the actual ones, by averaging their values along the measuring path, as the following expression (number (10) from Ref. [15]) indicates:

$$\hat{u}_i^{\mathrm{M}}(\boldsymbol{x}, l) = \frac{1}{l} \int_{-l/2}^{l/2} \hat{u}_i(\boldsymbol{x} + \boldsymbol{p}) \, \mathrm{d}p. \tag{39}$$

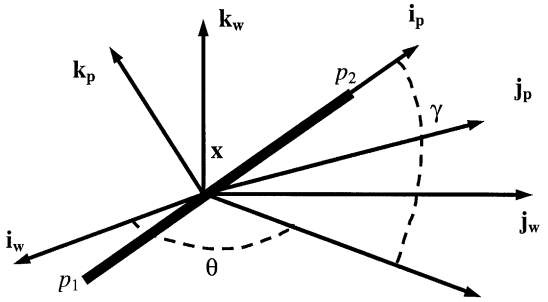

Fig. 4. Measuring path p_1–p_2 and reference systems: wind ($\boldsymbol{i}_w$, $\boldsymbol{j}_w$, $\boldsymbol{k}_w$) and ($\boldsymbol{i}_p$, $\boldsymbol{j}_p$, $\boldsymbol{k}_p$) path reference systems, respectively.

In the above-mentioned papers the line-averaging process is considered as instantaneous. As it has been shown in previous paragraphs in fact, it is not. If one considers that each ultrasonic pulse needs a time to complete each traverse between transducers, additional effects to the one described by the line-averaging model are found. These effects depend on the ratio of the averaged wind speed to the sound speed, the Mach number of the flow.

Let us consider a single measuring path inside an atmospheric three-dimensional, non-steady, non-uniform wind speed field. This wind speed field will be expressed, from now on, by its averaged value $\boldsymbol{u}_\infty$ and its turbulent components with zero mean $\hat{u}_i(\boldsymbol{x}, t)$, as follows:

$$u_i(\boldsymbol{x}, t) = \boldsymbol{u}_\infty + \hat{u}_i(\boldsymbol{x}, t). \tag{40}$$

The center of the measuring path is located at a point $\boldsymbol{x}$, and angles θ and γ are used to define its direction. Fig. 4 represents the situation of the path and the different reference systems. Two reference systems are defined: First ($\boldsymbol{i}_w$, $\boldsymbol{j}_w$, $\boldsymbol{z}_w$) the mean wind speed reference system, commonly used in meteorology, and second ($\boldsymbol{i}_p$, $\boldsymbol{j}_p$, $\boldsymbol{z}_p$) the reference system associated with the measuring path. $\boldsymbol{i}_w$ is aligned with the mean wind speed whereas $\boldsymbol{i}_p$ is aligned with the direction p_1–p_2 of the measuring path.

Assuming as valid the hypothesis stated in the appendix, the pulse speed to be considered in the calculations is the projection along the measuring path given by

$$u_p(\boldsymbol{x}, t) = \boldsymbol{u}(\boldsymbol{x}, t) \cdot \boldsymbol{i}_p \pm c, \tag{41}$$

where $\pm$ corresponds to the pulse travelling from p_1 to p_2 and p_2 to p_1, respectively. The scalar product $\boldsymbol{u}(\boldsymbol{x}, t) \cdot \boldsymbol{i}_p$ gives

$$\boldsymbol{u}(\boldsymbol{x}, t) \cdot \boldsymbol{i}_p = c_1[|\boldsymbol{u}_\infty| + \hat{u}_1(\boldsymbol{x}, t)] + c_2\hat{u}_2(\boldsymbol{x}, t) + c_3\hat{u}_3(\boldsymbol{x}, t). \tag{42}$$

The coefficients c_i are as follows:

$$c_1 = \cos\theta\cos\gamma, \quad c_2 = \sin\theta\cos\gamma, \quad c_3 = \sin\gamma. \tag{43}$$

In this case, slightly different reference values are defined in the process of converting dimensional magnitudes into non-dimensional ones. Although a speed reference value associated with the measuring path would be $c_1|\boldsymbol{u}_\infty|$, it could produce

some problems if the measuring path lies in the $\boldsymbol{j}_w$ or z_w direction. It both cases u_r would be 0 and the non-dimensional speed would be undefined. This is the reason why in this case the following reference values are used:

$$u_r = |\boldsymbol{u}_\infty|, \quad M_r = M_\infty = \frac{|\boldsymbol{u}_\infty|}{c}. \tag{44}$$

Considering the previous values, the term $\varepsilon\,\delta(p,t)$ defined in Eq. (9) results in this case:

$$\varepsilon u_r \delta(\boldsymbol{x},p,t) = c_i \hat{u}_i(\boldsymbol{x},p,t), \tag{45}$$

where Einstein's notation has been considered to denote the summation $\sum_{i=1}^{i=3} c_i\hat{u}_i$.

The equations defined in Eqs. (10a), (10b) and (20) change slightly due to the special definition of reference systems. In this case they result as follows:

$$\begin{gathered} \mathrm{d}T^{\pm}(\boldsymbol{x},T,P) = \pm \frac{M_\infty/(1 \pm c_1 M_\infty)\,\mathrm{d}P}{1 \pm M_\infty/(1 \pm c_1 M_\infty)\, c_i \hat{U}_i(\boldsymbol{x},P,T)}, \\ T^{\pm}(\boldsymbol{x},0) = 0, T_{21},\ T^{\pm}(\boldsymbol{x},1) = T_{12}, 0. \end{gathered} \tag{46}$$

It should be noted that the dependence of the functions with the spatial location $\boldsymbol{x}$ has been included. This vector locates the centre of the measuring path, and all wind speed measurements will be referred to this position.

In non-dimensional terms, the measuring path extends from 0 to 1 (p_1–p_2). In order to make easy the comparison of the results with the ones already established in the literature, this path is redefined to the interval $[-\frac{1}{2}, \frac{1}{2}]$. Thus Eqs. (15) and (23) become:

$$T_0^{\pm}(P) = \frac{M_\infty}{1 \pm c_1 M_\infty}\left(\frac{1}{2} \pm P\right). \tag{47}$$

Finally the expression for the total time of flight in both shots, given by Eqs. (18) and (21) results in

$$T_{12}(\boldsymbol{x}) = \frac{M_\infty}{1 + c_1 M_\infty}\left(1 - \frac{M_\infty}{1 + c_1 M_\infty}\,\varepsilon F^{+}(\boldsymbol{x})\right), \tag{48a}$$

$$T_{21}(\boldsymbol{x}) = \frac{M_\infty}{1 - c_1 M_\infty}\left(1 + \frac{M_\infty}{1 - c_1 M_\infty}\,\varepsilon F^{-}(\boldsymbol{x})\right). \tag{48b}$$

In the atmospheric case the term ε which includes the order of magnitude of the disturbing terms of wind speed is intrinsically included in the specific formulation as it appears in Eq. (45). Following the procedure described before, expressions (19) and (22) become

$$\varepsilon F^{\pm}(\boldsymbol{x}) = \int_{-1/2}^{1/2} c_i \hat{U}_i(\boldsymbol{x},P,T_0^{\pm}(P))\,\mathrm{d}P. \tag{49}$$

Introducing Eqs. (48a) and (48b) in Eq. (7) gives rise to

$$U_{\mathrm{p}}^{\mathrm{M}}(\boldsymbol{x}) = c_1 + \tfrac{1}{2}\,(\varepsilon F^{+}(\boldsymbol{x}) + \varepsilon F^{-}(\boldsymbol{x})). \tag{50}$$

The turbulent atmospheric wind speed field can be defined through a Fourier-Stieltjes integral, see Refs. [15] or [19]:

$$\hat{u}_i(\boldsymbol{x}, t) = \int_{-\infty}^{\infty} \mathrm{e}^{\mathrm{i}\boldsymbol{k}\cdot\boldsymbol{x}}\, \mathrm{d}\Psi_i(\boldsymbol{k}, t), \tag{51}$$

where $\boldsymbol{k}$ has been previously defined as the wave-number vector with components k_1, k_2 and k_3 along the co-ordinate directions $\boldsymbol{x}_{\mathrm{w}}$, $\boldsymbol{y}_{\mathrm{w}}$ and $\boldsymbol{z}_{\mathrm{w}}$, and $\Psi_{\mathrm{i}}(\boldsymbol{k}, t)$ are random functions with orthogonal increments

$$\overline{\mathrm{d}\Psi_i(\boldsymbol{k}, t)\, \mathrm{d}\Psi_j^{*}(\boldsymbol{k}', t)} = \begin{cases} 0, & \boldsymbol{k} \neq \boldsymbol{k}', \\ \Phi_{ij}(\boldsymbol{k})\, \mathrm{d}\boldsymbol{k}, & \boldsymbol{k} = \boldsymbol{k}', \end{cases} \tag{52}$$

where the asterisk indicates complex conjugate and the over-bar denotes averaging. $\Phi_{ij}(\boldsymbol{k})$ is the spectral density tensor. It can present several forms, depending on the assumptions. In case of isotropy it can be expressed as follows:

$$\Phi_{ij}(\boldsymbol{k}) = \frac{E(k)}{4\pi k}\,(k^2\delta_{ij} - k_i k_j), \tag{53}$$

where $E(k)$ is the so-called three-dimensional spectrum and k is the magnitude of $\boldsymbol{k}$. If an inertial sub-range exists in the wave-number range of interest, according to the Von Karman's model [19]

$$E(k) \propto \in^{2/3}\ k^{-5/3}, \tag{54}$$

where $\in$ is the rate of turbulent energy dissipation.

Following Ref. [15], what are usually available from measurements using Taylor's hypothesis are the components of the one-dimensional spectral density tensor. This tensor is the Fourier transform of the velocity correlation tensor for separation in the longitudinal ($\boldsymbol{x}_{\mathrm{w}}$) direction. Denoting this one-dimensional spectral density tensor as $F_{ij}(k_1)$ we have

$$F_{ij}(k_1) = \int_{-\infty}^{\infty}\int_{-\infty}^{\infty} \Phi_{ij}(\boldsymbol{k})\, \mathrm{d}k_2\, \mathrm{d}k_3. \tag{55}$$

Expression (55) will be used from now on to establish comparisons between real and measured values.

Taylor hypothesis of frozen turbulence is considered, so that the turbulent flow will be interpreted as a non-uniform spatial pattern that moves with speed $\boldsymbol{u}_{\infty}$. This essentially means that at a point $\boldsymbol{x}$ at time $t_{\mathrm{r}} + t$ there is the same wind speed than at the point $x - \boldsymbol{u}_{\infty} t$ at time t_{r}. Thus, it can be written as

$$\hat{u}_i(\boldsymbol{x}, P, t, l) = \hat{u}_i(\boldsymbol{x} + Pl\boldsymbol{i}_{\mathrm{p}} - |\boldsymbol{u}_{\infty}|\ t\ \boldsymbol{i}_{\mathrm{w}}). \tag{56}$$

Eq. (56) will be used to find the value of $\hat{u}_i$ along the measuring path, given by Pl with reference to point $\boldsymbol{x}$, after a given time t has elapsed. It should be noted that the reference time is $t_{\mathrm{r}} = 0$. Considering any other values for t_{r} other than 0 will not make any difference.

The time of arrival of the pulses at a given position P in both back and forth pulse travels in the first approximation are given by Eq. (47). Therefore the turbulent components along the measurement paths seen by both pulses are obtained by substituting Eq. (47) in Eq. (56), that is

$$\hat{u}_i^{\pm}(\boldsymbol{x}, P, l) = \hat{u}_i^{\pm}(\boldsymbol{x} + Pl \cdot \boldsymbol{i}_{\mathrm{p}} - (T_0^{\pm}(P)\, l + \upsilon(\pm) Z_{\mathrm{B}} l) \cdot \boldsymbol{i}_{\mathrm{w}}), \tag{57}$$

where Z_{B} represents the non-dimensional delay time between pulse shots and $\upsilon(\pm)$ is a function of the sign defined as $\upsilon(+) = 0$, $\upsilon(-) = 1$. Now making Eq. (57) non-dimensional, expressing them in the form (51), one gets

$$\hat{U}_i^{\pm}(\boldsymbol{x}) = \frac{1}{|\boldsymbol{u}_\infty|} \times \int_{-\infty}^{\infty} \exp\left\{ \mathrm{i}\boldsymbol{k} \cdot \left[\boldsymbol{x} + Pl\boldsymbol{i}_{\mathrm{p}} - \left[\frac{M_\infty}{1 \pm c_1 M_\infty} \left(\frac{1}{2} \pm P \right) l + \upsilon(\pm) Z_{\mathrm{B}} l \right] \boldsymbol{i}_{\mathrm{W}} \right] \right\} \mathrm{d}\Psi_i(\boldsymbol{k}, t). \tag{58}$$

The functions εF^+ and εF^-, defined in Eq. (49), will have the following expressions:

$$\varepsilon F^{\pm}(\boldsymbol{x}, \boldsymbol{k}, M_\infty, c_i, l, Z_{\mathrm{B}}) = \int_{-1/2}^{1/2} c_i\, \hat{U}_i^{\pm}(\boldsymbol{x}, \boldsymbol{k}, P, M_\infty, c_1, l, Z_{\mathrm{B}})\, \mathrm{d}P. \tag{59}$$

By introducing Eq. (58) in Eq. (59) the following expressions are obtained:

$$\varepsilon F^{\pm} = \frac{1}{|\boldsymbol{u}_\infty|} \times \int_{-1/2}^{1/2} c_i \left\{ \int_{-\infty}^{\infty} \exp\left\{ \mathrm{i}\boldsymbol{k} \cdot \left[\boldsymbol{x} + Pl\, \boldsymbol{i}_{\mathrm{p}} - \left[\frac{M_\infty}{1 \pm c_1 M_\infty} \left(\frac{1}{2} \pm P \right) l + \upsilon(\pm) Z_{\mathrm{B}} l \right] \boldsymbol{i}_{\mathrm{W}} \right] \right\} \times \mathrm{d}\Psi_i(\boldsymbol{k}, t) \right\} \mathrm{d}P. \tag{60}$$

Interchanging the integration order and operating:

$$\varepsilon F^{\pm} = \frac{1}{|\boldsymbol{u}_\infty|} \int_{-\infty}^{\infty} c_i \exp(\mathrm{i}\boldsymbol{k} \cdot \boldsymbol{x}) \times \left\{ \int_{-1/2}^{1/2} \exp\left[\mathrm{i}\boldsymbol{k} \cdot \boldsymbol{i}_{\mathrm{p}} Pl - i \left[\frac{M_\infty}{1 \pm c_1 M_\infty} \left(\frac{1}{2} \pm P \right) + \upsilon(\pm) Z_{\mathrm{B}} \right] k_1 l \right] \mathrm{d}P \right\} \mathrm{d}\Psi_i(\boldsymbol{k}, t). \tag{61}$$

Solving the inner integrals we get

$$\varepsilon F^{\pm} = \frac{1}{|\boldsymbol{u}_\infty|} \int_{-\infty}^{\infty} c_i \exp\,(\mathrm{i}\boldsymbol{k} \cdot \boldsymbol{x}) G^{\pm}\, \mathrm{d}\Psi_i(\boldsymbol{k}, t), \tag{62}$$

where G^+ and G^- are

$$G^{\pm} = \exp\left(-\frac{i}{2}\frac{M_\infty k_1 l}{1 \pm c_1 M_\infty} - \mathrm{i}\upsilon(\pm) Z_B k_1 l\right) \times \left[\frac{\sin\left((\boldsymbol{k}\cdot\boldsymbol{i}_p l)/2 \mp 1/2\ (M_\infty k_1 l)/(1 \pm c_1 M_\infty)\right)}{(\boldsymbol{k}\cdot\boldsymbol{i}_p l)/2 \mp 1/2\ (M_\infty k_1 l)/(1 \pm c_1 M_\infty)}\right]. \tag{63}$$

The measured speed U_p^M defined in Eq. (50) is obtained by using Eqs. (62) and (63):

$$u_p^M(\boldsymbol{x}, l,\ M_\infty, c_i) = c_1|\boldsymbol{u}_\infty| + \frac{1}{2}c_i \int_{-\infty}^{\infty} \exp(\mathrm{i}\boldsymbol{k}\cdot\boldsymbol{x})\ [G^+(\boldsymbol{k}, l, M_\infty, c_1) + G^-(\boldsymbol{k}, l, M_\infty, c_i, Z_B)]\ \mathrm{d}\Psi_i(\boldsymbol{k}). \tag{64}$$

Let us consider now the second term of the right-hand side of Eq. (64) to be a new turbulent speed field. Thus, it can be expressed as follows:

$$\hat{u}_p^M(\boldsymbol{x}, L, M_\infty, c_i) = \int_{-\infty}^{\infty} \exp(\mathrm{i}\boldsymbol{k}\cdot\boldsymbol{x})\ \mathrm{d}\Psi_p^M(\boldsymbol{k}, L, M_\infty, c_i). \tag{65}$$

Now after comparing Eqs. (64) and (65) one can obtain the following relation:

$$\mathrm{d}\Psi_p^M(\boldsymbol{k}, L, M_\infty, c_i) = \tfrac{1}{2}c_i\ [G^+(\boldsymbol{k}, L, M_\infty, c_i) + G^-(\boldsymbol{k}, L, M_\infty, c_i, Z_B)] d\Psi_i(\boldsymbol{k}). \tag{66}$$

A simple case can now be commented. Let us suppose that the measuring path lies along the $\boldsymbol{x}_w$ direction. In this conditions $c_1 = 1$ and $c_2 = c_3 = 0$. Thus Eq. (66) can be written as follows:

$$\mathrm{d}\Psi_1^M = \mathrm{d}\Psi_p^M\ (\boldsymbol{k}, l, M_\infty) = \tfrac{1}{2}\ [G^+(\boldsymbol{k}, l,\ M_\infty) + G^-(\boldsymbol{k}, l, M_\infty, Z_B)]\ \mathrm{d}\Psi_1(\boldsymbol{k}). \tag{67}$$

Considering now Eq. (52), functions Φ_{11}^M and Φ_{11} are calculated

$$\Phi_{11}^M\ \mathrm{d}\boldsymbol{k} = \overline{\mathrm{d}\Psi_1^M(\boldsymbol{k})\ [\mathrm{d}\Psi_1^M(\boldsymbol{k})]^*} = \frac{1}{4}\ [G^+ + G^-]\ [G^+ + G^-]^*\ \Phi_{11}\ \mathrm{d}\boldsymbol{k}. \tag{68}$$

The real and measured one-dimensional spectra can be calculated from Eq. (68) taking into account Eq. (55):

$$F_{11}(k_1) = \int_{-\infty}^{\infty}\int_{-\infty}^{\infty} \Phi_{11}(k_1, k_2, k_3)\ \mathrm{d}k_2\ \mathrm{d}k_3,$$

$$F_{11}^M(k_1) = \int_{-\infty}^{\infty}\int_{-\infty}^{\infty} \Phi_{11}^M(k_1, k_2, k_3)\ \mathrm{d}k_2\ \mathrm{d}k_3. \tag{69}$$

The method proposed in Ref. [15] is applied to establish the effect of the measurement. It consists in calculating the ratio $R_{ij}(k_1)$ as follows:

$$R_{ij}(k_1) = \frac{F_{ij}^M(k_1)}{F_{ij}(k_1)}, \tag{70}$$

where Einstein's notation has not been applied here.

Since F_{11} and F_{11}^{M} do neither depend on k_2 nor k_3, one can easily write

$$R_{11}(k_1, l, M_\infty, Z_\mathrm{B}) = \frac{F_{11}^{\mathrm{M}}(k_1, l, M_\infty, Z_\mathrm{B})}{F_{11}(k_1)} = \frac{1}{4}[G^+ + G^-][G^+ + G^-]^*. \tag{71}$$

Finally, introducing the particularised expressions (63) in Eq. (71), the transfer function R_{11} can be obtained. As it is clarified in Kaimal 1978, R_{11} is not, properly said, a transfer function, since a specific model for the wind has been considered. In spite of that, it allows the effect of the measuring algorithm to be analysed

$$R_{11}(k_1, L, M_\infty, Z_\mathrm{B}) = \frac{1}{4} \times \left\{ \sin c(+)^2 + \sin c(-)^2 + 2\cos\left[k_1 l \left(\frac{M_\infty^2}{(1 - M_\infty)^2} + Z_\mathrm{B}\right)\right] \sin c(+) \sin c(-) \right\}, \tag{72}$$

where

$$\sin c(\pm) = \frac{\sin((k_1 l/2)\ 1/(1 \pm M_\infty))}{(k_1 l/2)\ 1/(1 \pm M_\infty)}. \tag{73}$$

This expression should be compared with expression (15) in Ref. [15]. It must be remarked that Eq. (72) becomes expression (15) from Ref. [15] if both M_∞ go to 0 (c go to ∞ compared to $|\boldsymbol{u}_\infty|$) and no delay between pulse shots exists. These assumptions have been traditionally considered in line-averaging models. The model proposed here offers the possibility of analysing both effects, M_∞ which represents the fact that pulses need a finite time to do the flight, and the mentioned delay Z_B. Always considering that wind speed at a specific point is continuously changing.

The results obtained with Eq. (72) for the different Mach numbers are shown in Fig. 5 the results for R_{11} obtained by the instantaneous line average [15] are recovered when M_∞ goes to 0, and as M_∞ increases, the low-pass cut value for the parameter $k_1 l$ decreases.

The effect of the delay is quite noticeable (Fig. 6). Delays as small as $z_\mathrm{B} = 0.005$ s ($Z_\mathrm{B} = 1.154$) in a normal operation case for a sonic anemometer with $l = 0.15$ m, operating in air at a temperature of 298 K and therefore $c = 346.03$ m/s ($M_\infty = 0.1$ at $|\boldsymbol{u}_\infty| = 34.6$ m/s) lead to a low pass cut value for the wave-number parameter $k_1 l$ decreasing from $k_1 l = 2.14$ to 0.93.

The consideration of M_∞ and Z_B in the model changes the value $k_1 l = 1$ stated by Kaimal as the limit value for influence of line-averaging effect in the measurement of turbulent wind speed by sonic anemometers. The limit value for $k_1 l$ is significantly reduced down to values of about $k_1 l = 0.77$ for $M_\infty = 0.4$ or about $k_1 l = 0.1$ for a non-dimensional time delay $Z_\mathrm{B} = 2.307$.

Another case, usually analysed, consists of the measurement of turbulent velocities along z_w when the measuring path has the same direction. In this case $c_3 = 1$ and $c_1 = c_2 = 0$, and the "transfer function" R_{33} becomes

$$R_{33} = \frac{1/4 \int_{-\infty}^{\infty} \int_{-\infty}^{\infty} [G^+ + G^-]\,[G^+ + G^-]^*\, \Phi_{33}\, \mathrm{d}k_2\, \mathrm{d}k_3}{\int_{-\infty}^{\infty} \int_{-\infty}^{\infty} \Phi_{33}\, \mathrm{d}k_2\, \mathrm{d}k_3}. \tag{74}$$

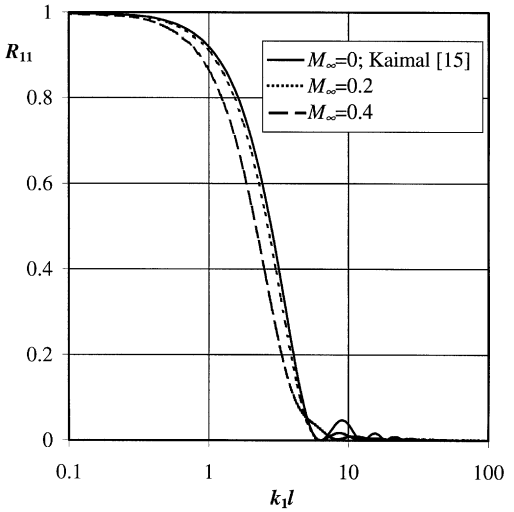

Fig. 5. Variation of the "transfer function R_{11}" with the wave-number parameter $k_1 l$ for different values of the Mach number M_∞. $Z_B = 0$. Kaimal's line-averaging model result is included as reference.

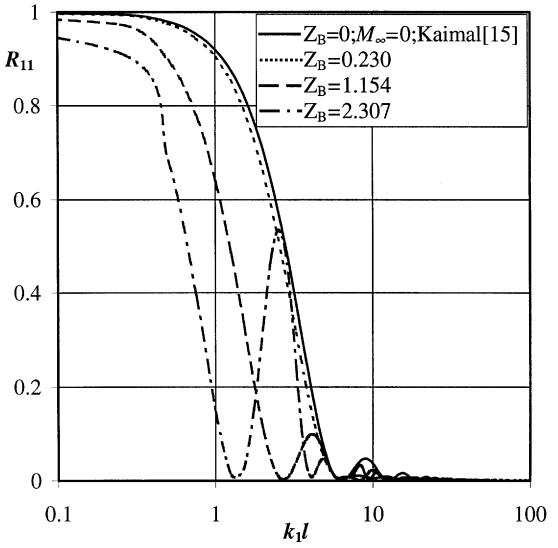

Fig. 6. Variation of the "transfer function R_{11}" with the wave-number parameter $k_1 l$ for different values of dimensionless time delay Z_B. $M_\infty = 0.1$. Kaimal's line-averaging model result is included as reference.

R_{33} case is not as simple as R_{11} since Φ_{33}, G^+ and G^- depend on k_3. In this case, the term $[G^+ + G^-][G^+ + G^-]^*$ gives the following expression:

$$[G^+ + G^-]\,[G^+ + G^-]^* = \sin d(+)^2 + \sin d(-)^2 + 2\cos(k_1 l Z_B)\sin d(+)\sin d(-) \tag{75}$$

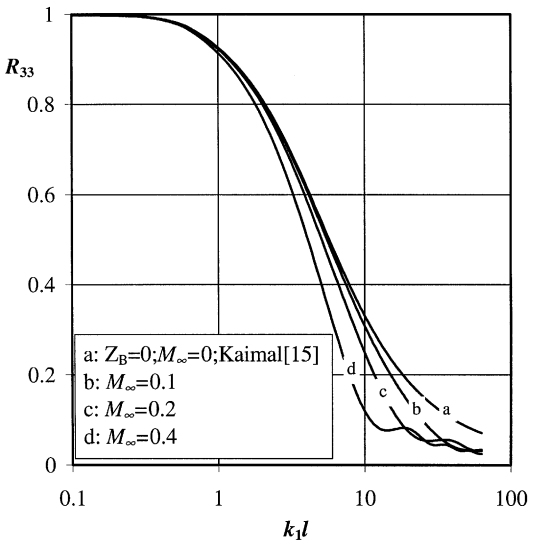

Fig. 7. Variation of the "transfer function R_{33}" with the parameter $k_1 l$ for different values of Mach number M_∞, Dimensionless time delay $Z_B = 0$. Kaimal's line-averaging model result is included as reference.

where

$$\sin d(\pm) = \frac{\sin\left[l/2\ (k_3 \pm M_\infty k_1)\right]}{l/2\ (k_3 \pm M_\infty k_1)}\,. \tag{76}$$

It should be noted again that Eq. (74) becomes expression (15) from Ref. [15] when both M_∞ and Z_B go to 0.

As shown in Fig. 7 function R_{33} approaches to Kaimal's line averaging results as M_∞ goes to 0. On the other hand, as M_∞ increases, the low pass cut value for $k_1 l$ decreases (i.e. at $k_1 l = 9.01$, R_{11} ranges from 0.36 at $M_\infty = 0$ up to 0.15 at $M_\infty = 0.4$). Fig. 8 shows that Z_B effect is noticeable. For the same situation as for evaluation of R_{11} the low pass cut value for the wave-number parameter $k_1 l$ decreases from $k_1 l = 3.34$ to 0.94.

Mean wind speed presents an important influence in the attenuation of Φ_{11} measurement. Fig. 9 is included to illustrate this statement. In it, the response of two commercial anemometer sonic paths operating in air (normal conditions) is displayed, for a time delay $z_B = 0$ s. The attenuation at low mean wind speed is higher, because at the same frequency of turbulent speed, the number of speed oscillation cycles within the path l is larger. At mean wind speed values of about 10 m/s, attenuation factors of some 10% can be observed at 10 Hz. The effect of the path length can be analysed in the same way, thus for both a given mean wind speed and frequency, a larger path induces larger attenuation factors, since the number of speed oscillation cycles occurring along the measurement path is again larger. At a given wind speed and frequency, the differences in length studied in the example lead to differences in the attenuation factor up to 20% for higher frequencies.

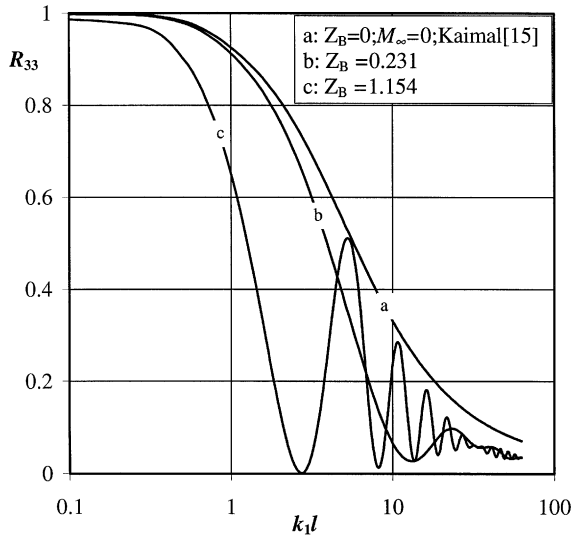

Fig. 8. Variation of the "transfer function R_{33}" with the parameter $k_1 l$ for different values of Dimensionless time delay Z_B, Mach number $M_\infty = 0.1$. Kaimal's line-averaging model result is included as reference.

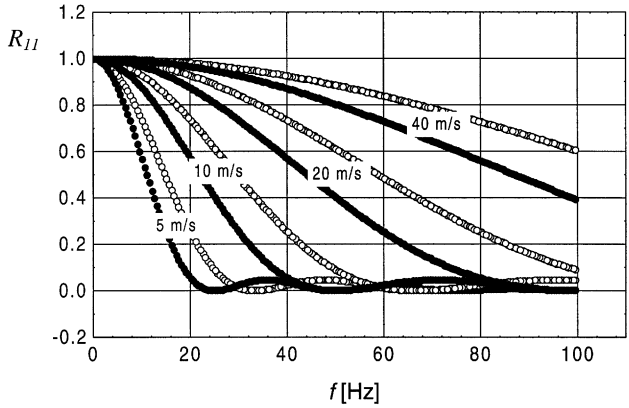

Fig. 9. Variation of the "transfer function R_{11}" with frequency of turbulent wind speed. Sonic paths operating in air at normal conditions. Time delay $z_B = 0$ s. Filled dots: Kaijo Denki, ($l = 0.20$ m). Empty dots: Gill WindMaster, $l = 0.15$ m.

Both time delay, z_B and path length l, induce significant differences in the attenuation factor for Φ_{11} measurement (Fig. 10). For a given path of $l = 0.15$ m operating in air at normal conditions and a mean wind speed of 25 m/s, a time delay difference from $z_B = 0.0005$ to 0.005 s leads to differences in the attenuation factor up to 3% for frequencies at some 10 Hz or 42% for frequencies at some 60 Hz. For a given time delay $z_B = 0.0005$, the differences in the attenuation due to the path length

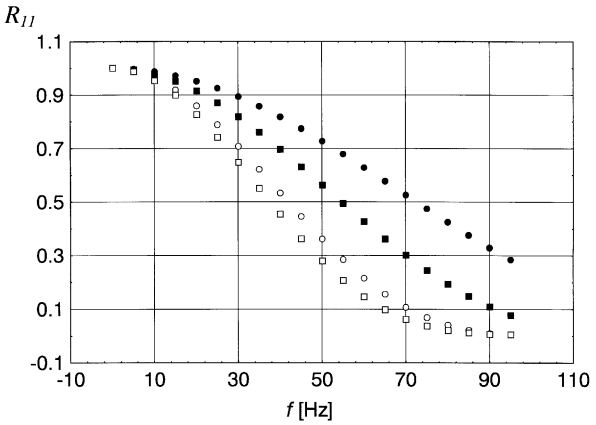

Fig. 10. Variation of the "transfer function R_{11}" with frequency of turbulent wind speed. Sonic paths operating in air at normal conditions, $u_\infty = 25$ m/s. Filled dots: Time delay $z_B = 0.0005$ s. Empty dots: Time delay $z_B = 0.005$ s. Circles: Gill WindMaster ($l = 0.15$ m.). Squares: Kaijo Denki ($l = 0.20$ m).

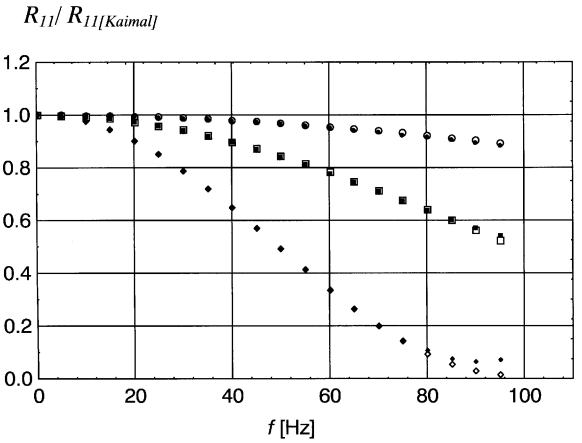

Fig. 11. Ratio of "transfer function R_{11}" predicted by the model presented to the one proposed by "Line averaging model" (Kaimal's model) for three values of Time delay z_B. Sonic paths operating in air at normal conditions, $u_\infty = 25$ m/s. Filled dots: Kaijo Denki ($l = 0.20$ m.). Empty dots: Gill WindMaster ($l = 0.15$ m.). Circles: Time delay $z_B = 0.001$ s. Squares: Time delay $z_B = 0.0025$ s. Rhombuses: Time delay $z_B = 0.005$ s.

reach values of some 1% for frequencies about 10 Hz or values of some 20% for frequencies about 60 Hz. The attenuation factors corresponding to the smaller path are always lesser due, again, to the presence of a smaller number of wind speed oscillation cycles. The difference induced by the length of the path is smaller for the higher time delay z_B, within all the frequency range considered.

Fig. 11 shows the correction obtained from the proposed model in terms of the ratio of the transfer function calculated using the new model to the one calculated

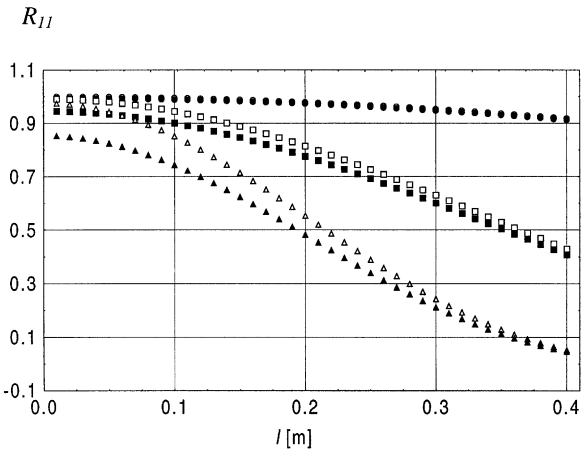

Fig. 12. Variation of the "transfer function R_{11}" with path length l. Sonic paths operating in air at normal conditions, $u_\infty = 25$ m/s. Empty dots: Time delay $z_B = 0.001$ s. Filled dots: Time delay $z_B = 0.005$ s. Circles: Turbulent speed frequency $f = 10$ Hz. Squares: Turbulent speed frequency $f = 30$ Hz. Triangles: Turbulent speed frequency $f = 50$ Hz.

from Ref. [15] corresponding to the "line-averaging" model. The example is calculated for two sonic paths operating again in a atmospheric flow (air at normal conditions) with 25 m/s mean wind speed. The results are presented for three different time delays z_B. The proposed model provides corrections for the attenuation factor of the measurement of Φ_{11} that range from values less than 1% for frequencies at about 5 Hz for all time delays z_B up to corrections at about 90 Hz that reach values of 10, 40 and 92% for time delays z_B of 0.001, 0.0025 and 0.005 s, respectively. The path length does not have a relevant influence on the corrections.

Fig. 12 presents the influence of path length at three different frequencies of turbulent wind speed, f, and two values of Time delay z_B. The effect of the path is much more significant at higher frequencies since the ultrasound pulse experiences a higher number of wind speed oscillation cycles.

8. Conclusions

A general revision of sonic measurement theory, derived from the solution of the differential equations that describe the flight of the ultrasound pulses, has been presented. Both the spatial and time variations of flow speed field induce differences between the measured speed and the instantaneous space average along the measurement path, which is against the classical assumption.

A general expression for this difference has been obtained, showing a dependency, in the first approximation, on the Mach number of the flow and therefore on fluid flow characteristics such as its composition or temperature. It also depends on the time delay between pulse shots.

In a non-steady, uniform flow field, a workable solution is found for harmonic variations. An example of a sonic path installed on an oscillating met. mast is analysed to illustrate the effect. Generally speaking errors are significant for dimensionless angular frequencies $\Omega > 1$ and for Mach number $M_r > 0.1$. Notwithstanding that, corrective actions are mentioned to compensate for these effects. Expressions for the error induced by the delay between back and forth pulse shots are also obtained. The relative errors could amount to 10^{-2}.

In the case of a non-uniform, steady flow field, flow non-uniformity has been found to have much less influence on the sonic anemometer measurements (typical relative error 10^{-4}) than in the case of cup anemometers where non-uniformity larger than 0.2% should be avoided during calibrations. These results are also interesting from the point of view of the elaboration of wind tunnel calibration flow quality requirements.

Three-dimensional atmospheric flow is analysed as representative of a non-steady, non-uniform flow field. The influence of Mach number, as well as the time delay between pulse shots, on wind speed spectral measurements is not negligible. The value $k_1 l = 1$, established by Kaimal [15] as the limit for influence of the line-averaging process on the measurement with sonic anemometers must be reviewed when Mach number M, and Time delay Z_B are considered in the new model. The correction over the line-averaging models existing in the literature cannot be neglected, i.e. the value for the attenuation of the longitudinal spectrum at $k_1 l = 1$ decreases by some 5% when one considers $M = 0.4$ or by some 76% for a non-dimensional time delay $Z_B = 2.307$ (compared with the Kaimal estimation). Line-averaging model results are recovered when Mach number and time delay between pulses go to 0 in the model proposed here.

Two commercial sonic paths operating in air at normal conditions are investigated over a wide frequency interval, for different wind speeds and time delays. The path length is proven to have an important influence on the attenuation of the measurement, as well as the time delay, specially for higher frequencies. The specific influence of Mach number and time delay (correction to the line averaging) can reach values up to 14% for the cases analysed. This is within 1% for frequencies lower than 10 Hz.

But more important than the numerical results corresponding to the practical cases shown, the model presented in this paper provides a simple mathematical tool to evaluate the influence of the most relevant factors in measurements with sonic anemometers.

This mathematical model can have several uses. For example the design of a sonic anemometer to a particular specification, sensitivity studies of sonic models, and the assessment of wind tunnel flow quality oriented to calibration or correction of experimental data.

Appendix A. Effect of a transversal wind speed component in the measurement

The common way of modelling the flight of pulses along the measuring path consists in considering the wind speed component along the path, and therefore

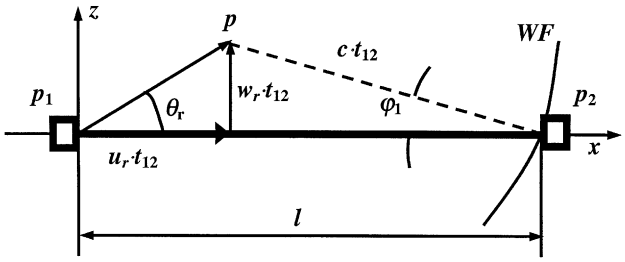

Fig. 13. Schematic figure to illustrate the flight of a pulse in an uniform and steady two dimensional flow field. WF: Sound wave front arriving at the receiver p_2.

considering that the pulse moves following the path line. In this part it will be shown that this is a good approximation, as stated in Ref. [2], and that its application leads to errors of order M_r^2.

A.1. Uniform, steady flow field

For this purpose a simplified geometry is considered, as well as a both uniform and steady two-dimensional wind speed field. See Fig. 13. The pulse travel can be considered the combination of a convection carried by the fluid from p_1 to p and a sound propagation in a fluid at rest from p to p_2

The wind speed along the path is u_r and the transversal values is w_r. The pulse is launched at time $t=0$ s from the path extreme p_1, and reach the extreme p_2 at time $t=t_{12}$. From the geometry described in Fig. 13, one can conclude that

$$u_r t_{12} + c\cos(\varphi_1)t_{12} = l. \tag{A.1}$$

Considering $M_r \ll 1$ then

$$\varphi_1 \ll 1 \Rightarrow \cos\varphi_1 \approx 1 - \frac{(\varphi_1)^2}{2}, \quad \sin\varphi_1 \approx \varphi_1 \approx \frac{w_r}{c}.$$

Also

$$\cos\varphi_1 \approx 1 - \frac{1}{2}\left(\frac{w_r}{c}\right)^2 \approx 1 - \frac{1}{2}M_r^2\left(\frac{w_r}{u_r}\right)^2 = 1 - \frac{1}{2}M_r^2\tan^2\theta_r. \tag{A.2}$$

The last expressions are valid when u_r is not 0. Using Eq. (A.2) in Eq. (A.1) the following expression can be obtained for t_{12}:

$$t_{12} = \frac{l}{u_r + c(1-(1/2)M_r^2\tan^2\theta_r)} \Rightarrow T_{12} = t_{12}\frac{u_r}{l}$$
$$= \frac{M_r}{1 + M_r - (1/2)M_r^2\tan^2\theta_r}. \tag{A.3}$$

Following a similar process for the pulse fight from p_2 to p_1, the following expression for T_{21} can be obtained:

$$T_{12} = \frac{M_r}{1 - M_r - (1/2)M_r^2 \tan^2 \theta_r}. \tag{A.4}$$

With the help of Eqs. (A.3) and (A.4) the measured speed U_p^M defined in Eq. (7) becomes

$$U_p^M = \frac{1}{2}\left(\frac{1}{T_{12}} - \frac{1}{T_{21}}\right) = 1. \tag{A.5}$$

From Eq. (A.5) it can be deduced that (in these conditions) the measuring process is exact, this is, the transversal component (to the path) of wind speed has no effect in the measurement of the wind speed component along the path, at least up to terms of order $O(M_r^2)$. This conclusion allows to solve the problem by first calculating the wind speed component along the path and afterwards solving Eqs. (4a) and (4b).

A.2. Non-uniform, non-steady flow field

The previous case is a simplified one, and a more general solution is often needed. Consider a general two-dimensional wind speed field (Fig. 14). The exact relationship for the pulse propagation displacement is

$$dt = \frac{dp}{c \cos \alpha + u_p(p, z, t)}, \tag{A.6}$$

where $p(t)$ and $z(t)$ are the co-ordinates of the pulse.

In order to evaluate the error involved in using $u_p(p(t), 0, t)$ instead of $u_p(p(t), z(t), t)$, the Taylor expansion of $u_p(p(t), z(t), t)$ in the neighbourhood of $z = 0$ is considered:

$$u_p(p, z, t) = u_p(p, 0, t) + z(t) \frac{\partial u_p(p, z, t)}{\partial z}|_{z=0} + O(z^2). \tag{A.7}$$

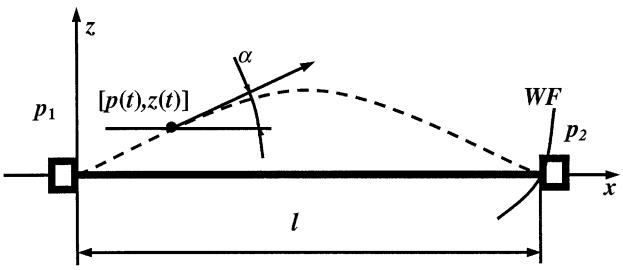

Fig. 14. Schematic of the trajectory of a sound pulse in a non-uniform, non-steady flow field. WF: Sound wave front arriving at the receiver p_2.

The contribution to the error in expression (4) employed in the paper comes from the second term in the R.H.S. of Eq. (A.7):

$$\Delta u_{\mathrm{p}} = z(t)\,\frac{\partial u_{\mathrm{p}}(p,z,t)}{\partial z}\Big|_{z=0}. \tag{A.8}$$

This term is 0 if there is not any lateral gradient of the longitudinal wind component u_{p}, this is $\partial u_{\mathrm{p}}/\partial z = 0$; and therefore no error occurs in this approximation for the uniform and steady flow fields in accordance with the results just obtained (A.5).

If $\partial u_{\mathrm{p}}/\partial z \neq 0$, then it is necessary to evaluate the contribution of this term. To do this it should be taken into account that $z(t)$ will be limited by its maximum value $z_{\max}$

$$z(t) \leqslant z_{\max} \approx \frac{w_{\mathrm{r}}}{c}\,l \tag{A.9}$$

and in dimensionless from

$$Z_{\max} = \frac{z_{\max}}{l} \approx \frac{w_{\mathrm{r}}}{c} = \frac{w_{\mathrm{r}}}{u_{\mathrm{r}}}\,M_{\mathrm{r}}\,. \tag{A.10}$$

Therefore the error is given by

$$\frac{\Delta u_{\mathrm{p}}}{u_{\mathrm{p}}} \approx \frac{w_{\mathrm{r}} l}{c l_Z} = \frac{w_{\mathrm{r}}}{u_{\mathrm{r}}}\,M_{\mathrm{r}}\,\frac{l}{l_Z}\,, \tag{A.11}$$

where l_Z is the characteristic length of the lateral variation of u_{p}. A more sound study of this source of errors requires a more detailed knowledge of the velocity field and the pulse trajectory, which are out of the scope of this paper. However, if the speed component u_{p} is given by a expression similar to Eq. (9) then

$$\frac{\partial u_{\mathrm{p}}}{\partial z} \approx \frac{u_{\mathrm{r}}}{l}\,\frac{\partial \delta}{\partial Z}\,\varepsilon \approx \frac{u_{\mathrm{r}}}{l_Z}\,. \tag{A.12}$$

As $\partial\delta/\partial Z = 0(1)$ hence $l_z \cong l/\varepsilon$. Furthermore, if the lateral component w_{r} is of the same order as u_{r} perturbations, then $w_{\mathrm{r}} \approx \varepsilon u_{\mathrm{r}}$ and from Eq. (A.11) the correction will be

$$\frac{\Delta u_{\mathrm{p}}}{u_{\mathrm{p}}} \approx \varepsilon^2 M_{\mathrm{r}}. \tag{A.13}$$

Therefore, in the cases considered in this paper, the results obtained from the model can be considered as correct at least to order $\varepsilon^2 M_{\mathrm{r}}$.

[1] V.E. Suomi, Sonic Anemometer, Exploring the Atmosphere's First Mile, Vol. 1, Instrumen. Soc Amer. Pergamon, New York, 1957, pp. 356–366.
[2] J.C. Kaimal, Sonic anemometer measurement of atmospheric turbulence, Proceedings of the Dynamic Flow Conference, 1978, pp. 551–565.
[3] J.C. Kaimal, J.C. Wyndgaard, The Kansas and Minnesota experiments, Boundary Layer Meteorol. 50 (1990) 31–47.
[4] N. Kato, T. Ohkuma et al., Full scale measurements of wind velocity in two urban areas using an ultrasonic anemometer, J. Wind Eng. Ind. Aerodyn. 41–44 (1992) 67–68.
[5] A. Cuerva, S. López, Identifying factors in wind turbine response by means of Principal Component Analysis, 18th ASME Wind Energy Symposium held with 37th AIAA Aerospace Sciences Meeting and Exhibit, Reno, Nevada, 1998.
[6] A. Fragoulis, The complex terrain wind environment and its effects on the power output and loading of wind turbines, 35th AIAA Aerospace Sciences Meeting and Exhibit, Reno, NV, January 6–9, Proceedings of 1997-97-0934, 1997, pp. 33–40.
[7] A. Fragoulis, A. Cuerva et al., MOUNTURB FINAL REPORT. Load and Power Measurement Program on Wind Turbines Operating in Complex Mountainous Regions, Vol. 2, CRES, Athens, 1996.
[8] J.C. Wyngaard, S. Zhang, Transducer-shadow effects on turbulence spectra measured by sonic anemometers, AMS, J. Atmos. Oceanic Technol. 2 (1985) 548–558.
[9] P.A. Coppin, An examination of cup anemometer overspeeding, Meteorol. Rdsh. 35 (1982) 1–11.
[10] A. Cuerva, A. Sanz-Andrés, Assessment of performances of ultrasonic anemometers as one step ahead in wind measurements of energy production of a wind turbine, Proceedings of EWEC 97, Dublin, 1997.
[11] S. Cervenca, Selection of anemometer for measurement of wind turbulence, ECN-I-92-029, DE92 557290, June 1992.
[12] A. Grelle, A. Lindroth, Flow distortion by a solent sonic anemometer: wind tunnel calibration and its assessment for flux measurement over forest and field, AMS J. Atmos. Oceanic Technol. 11 (1994) 1529–1542.
[13] C.B. Baker, Wind tunnel investigations of three sonic anemometers, Air Resources Laboratory, NOAA, Environmental Research Laboratories, PB90-149808, October 1989.
[14] N.G. Mortensen, Flow-response characteristics of the Kaijo Denki Omni-directional sonic anemometer (TR-61B), Risø National Laboratory, Roskilde, Denmark, Risø-R-704(EN), 1994.
[15] J.C. Kaimal, J.C. Wyndgaard, D.A. Haugen, Deriving power spectra from a three-component sonic anemometer, J. Appl. Meteorol. 7 (1968) 827–837.
[16] A.S. Gurvich, The pulsation spectra of the vertical component of wind velocity and their relations to the micrometeorological conditions, Izv. Atmos. Oceanic Phys. 4 (1962) 101–136.
[17] B.A. Silverman, The effect of spatial averaging on spectrum estimation, J. Appl. Meteorol. 7 (1968) 168–172.
[18] K. Henjes et al., Effect of pulse averaging on sonic anemometer spectra, J. Atmos. Oceanic Technol. (1998), submitted for publication.
[19] J. Mann, Models in micrometeorology, Risø National Laboratory, Roskilde, Denmark, Risø-R-727(EN), 1994.
[20] C.A. Friehe, Effects of sound speed fluctuations on sonic anemometer measurements, J. Appl. Meteorol. 15 (1976) 607–610.
[21] MEASNET, Measurement Procedure, Cup Anemometer Calibrations, Final Technical Experts Group Draft. 22/9-1997.